

THE EVOLUTION AND LUMINOSITY FUNCTION OF QUASARS FROM COMPLETE OPTICAL SURVEYS

Alexander Maloney^{1,2} and Vahé Petrosian^{3,4}

Center for Space Science and Astrophysics, Stanford University, Stanford, CA 94305

ABSTRACT

We use several quasar samples (LBQS, HBQS, Durham/AAT and EQS) to determine the density and luminosity evolution of quasars. Combining these different samples and accounting for varying selection criteria require tests of correlation and the determination of density functions for multiply truncated data. We describe new non-parametric techniques for accomplishing these tasks, which have been developed recently by Efron and Petrosian (1998). With these methods, the luminosity evolution can be found through an investigation of the correlation of the bivariate distribution of luminosities and redshifts. We use matter dominated cosmological models with either zero cosmological constant or zero spatial curvature to determine luminosities from fluxes. Of the two most commonly used models for luminosity evolution, $L \propto e^{kt(z)}$ and $L \propto (1+z)^{k'}$, we find that the second form is a better description of the data at all luminosities; we find $k' = 2.58$ ([2.14, 2.91] one σ region) for the Einstein - de Sitter cosmological model.

Using this form of luminosity evolution we determine a global luminosity function and the evolution of the co-moving density for the two types of cosmological models. For the Einstein - de Sitter cosmological model we find a relatively strong increase in co-moving density up to $z \lesssim 2$, at which point the density peaks and begins to decrease rapidly. This is in agreement with results from high redshift surveys. We find some co-moving density evolution for all cosmological models, with the rate of evolution lower for models with lower matter density. We find that the local cumulative luminosity function $\Phi(L_o)$ exhibits the usual double power law behavior. The luminosity density $\mathcal{L}(z) = \int_0^\infty L \Psi(L, z) dL$, where $\Psi(L, z)$ is the luminosity function, is found to increase rapidly at low redshift and to reach a peak at around $z \approx 2$. Our results for $\mathcal{L}(z)$ are compared to results from high redshift surveys and to the variation of the star formation rate with redshift.

Subject headings: Quasars, Luminosity Function, Cosmology

¹Departments of Physics and Mathematics

²email: maloney@bigbang.stanford.edu

³Departments of Physics and Applied Physics

⁴email: vahé@bigbang.stanford.edu

1. INTRODUCTION

Investigations of the evolution of the quasar population have played a major role in the development of our ideas about the nature of these sources and their connection to other extragalactic objects. Ever since the first complete survey of 3C radio quasars by Schmidt (1968) and the subsequent survey of 4C quasars by Lynds and Wills (1972) it has been evident that the population of quasars as a whole has undergone rapid evolution. Using the so-called $\langle V/V_{max} \rangle$ method these authors interpreted the evolution with redshift z as caused by an increase in the co-moving density of quasars with redshift. However, both the source counts (Giacconi et al. 1979, Tananbaum et al. 1979) and the redshift distribution of optically selected samples of quasars (see e.g. Marshall 1985) clearly showed that such pure density evolution (PDE) models, for which the luminosity function is separable as

$$\Psi(L, z) = \psi(L)\rho(z), \quad (1)$$

cannot be correct. As more data was accumulated the pure luminosity evolution (PLE) model, with

$$\Psi(L, z) = \psi(L/g(z))/g(z), \quad (2)$$

gained more popularity. The function $g(z)$ describes the luminosity evolution of the population and $L_o = L/g(z)$ is the luminosity adjusted to its present epoch ($z = 0$) value. This model, while providing a better fit to the data than that of pure density evolution, also appears to be inadequate in many cases (see e.g. Petrosian 1973, Schmidt and Green 1978, Koo and Kron 1988, Caditz and Petrosian 1990). Without loss of generality, we can write the luminosity function as

$$\Psi(L, z) = \rho(z)\psi(L/g(z), \alpha_i)/g(z). \quad (3)$$

With ψ normalized such that $\int_0^\infty \psi(L, \alpha_i) dL = 1$, $\rho(z)$ gives the density and its evolution and $\psi(L_o, \alpha_i)$ describes the local luminosity function (with $g(0) = 1$). Here we explicitly include the α_i , parameters such as spectral index and break luminosity that describe the shape of the luminosity function. In general, these parameters may vary with redshift. A surprising, and a priori unexpected, result has been the absence of evidence for strong shape variation.

Such results imply that the density and luminosity functions $\rho(z)$ and $g(z)$ describe the *physical evolution* of sources; e.g. the rate of birth and death of sources and the changes in source luminosity with time. Cavaliere and colleagues (see Cavaliere and Padovani 1988 and references cited therein) were the first to emphasize this fact. A more complete description of the relation between the physical evolution and the functions describing the generalized luminosity function (or statistical evolution) can be found in Caditz and Petrosian (1990). Unfortunately, this relation is not unique, thus any test of quasar models via their expected evolution with cosmic epoch must usually involve additional assumptions. For example, quasars could be long lived (compared to the Hubble time) sources created during a relatively short period at high redshift undergoing continuous luminosity evolution. This is the model used in Caditz, Petrosian and Wandel (1991). Alternatively, quasars

could be short lived phenomena with birth rate, death rate and luminosity that vary systematically with redshift (see Siemiginowska and Elvis 1997). Most of the work along these lines assumes what is now the standard model for the source of energy of quasars and other active galactic nuclei (or AGNs); namely, accretion onto a massive black hole.

Another interesting aspect of quasar evolution is the relation between the evolution of the luminosity density of quasars, $\mathcal{L} = \int L\Psi(L, z)dL$, and similar functions describing the evolution of galaxies, such as the star formation rate (SFR). As shown by the high redshift surveys of Schmidt et al. (1995) and others (e.g. Warren et al. 1994), the rapid rise with redshift of the luminosity of quasars stops around redshift 2 or 3 and is expected to drop, perhaps mimicking the SFR (see Shaver et al. 1998, Cavalieri and Vitorini 1998, and Hawkins and Véron 1996).

In this paper we determine the luminosity function and its evolution for combined samples of quasars from various surveys, described in §2. For a complete review of the various ways of accomplishing this task, see Petrosian (1992). We use here non-parametric methods based on Lynden-Bell's (1971) idea which was generalized by Efron and Petrosian (1992) to allow not only a determination of the functional forms but also a test of correlation between redshifts and luminosities. This is essential for any determination of the functional form of the luminosity evolution $g(z)$. The above papers deal with magnitude limited samples with only an upper magnitude (lower flux) limit. However, because of observational constraints, some of the samples are truncated in redshift space and some have an upper magnitude (lower flux) limit. The methods described in the above papers cannot be used for such multiply truncated data. New methods for treating this type of data were developed by Efron and Petrosian (1998). In §3 we describe these new techniques and their relation to the older methods. The choice of cosmological model also plays a crucial role in such determinations. It is well known that one can not determine both the evolution of the luminosity function and the parameters of the cosmological model from magnitude limited samples alone. Only by assuming values for the cosmological parameters such as matter density, curvature and cosmological constant can one calculate the form of $\Psi(L, z)$. Alternatively, with some assumptions about $\Psi(L, z)$ one can test various cosmological models. In §4 we describe the cosmological model parameters and in §5 we present the results of applications of the new statistical methods to the data described in §2. Finally, in §6 we summarize these results and present our conclusions.

2. THE DATA

There have been many surveys of quasars, ranging from the original radio selected samples of the 3C (Schmidt 1963) and 4C (Lynds and Wills 1972) surveys to a variety of other optically and X-ray selected samples. In this paper, we will focus only on optically selected data. We use data from four samples with relatively similar selection criteria that provide a somewhat homogeneous data set spanning a large area of the $L - z$ plane. In order to combine the samples, all magnitudes were transformed to the B band. Some of the samples were artificially truncated in order to insure completeness within the truncation limits. The combined sample consisted of 1552 objects in the

range $15.5 \lesssim B \lesssim 21.2$ and $0.3 < z < 2.2$, with well defined upper and lower magnitude limits for each object.

Figure 1 shows the distribution of the complete surveys in the $B - z$ plane, which at first sight shows little evidence for a Hubble relation of $B \propto 5 \log(z)$. However, as we shall discuss below, there is evidence for cosmological dimming with redshift of the sources.

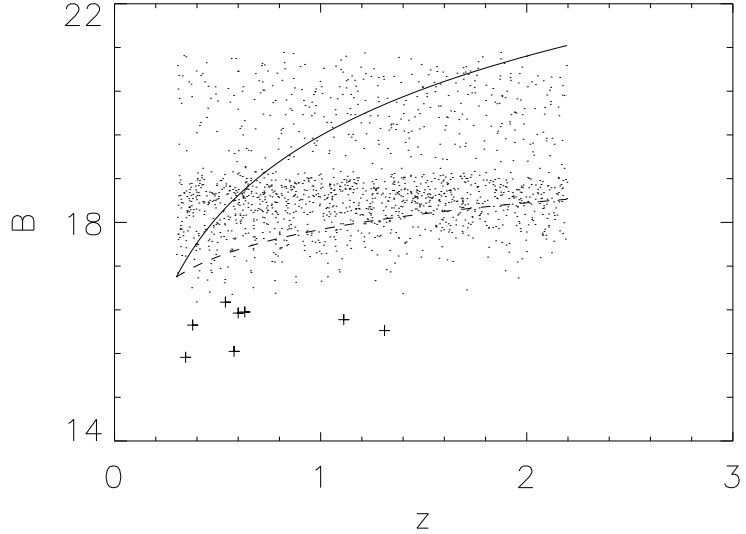


Fig. 1.— The B magnitude - redshift data for the four samples LBQS, HBQS, Durham/AAT and EQS described in §2, for $0.3 < z < 2.2$. The EQS data are marked with plus signs. The data are fitted to the parametric form $B(z) = B - \beta \log(d_L^2(z)K(z)) + \text{constant}$, where $d_L(z)$ is the luminosity distance and $K(z)$ is the K-correction term. The best fit ($\beta = 0.84$ for the Einstein - de Sitter cosmological model) is shown by the dashed line. The solid line shows the expected relation between B and z for standard candle sources without luminosity evolution ($\beta = 2.5$) in the Einstein - de Sitter model.

2.1. The Large Bright QSO Survey

The Large Bright QSO survey (LBQS) contains 1055 QSOs in the magnitude range $16.0 < B_J < 18.85$ and redshift range $0.2 < z < 3.4$ (Hewett et al. 1995). The faint magnitude limits for the 18 fields range from 18.41 to 18.85 and the bright magnitude limit is 16.0 for the entire sample. In order to transform from B_J to B magnitudes the color equation of Blair and Gilmore (1982)

$$B = B_J + 0.28(B - V) \quad (4)$$

was used assuming an average $B - V$ of 0.3 for the entire sample. When we combine this sample with the AAT sample and others we introduce artificial cutoffs at $z = 0.3$ and $z = 2.2$, which are the completeness limits for the AAT data. In addition, we removed all objects brighter than $B = 16.5$ in order to insure completeness near the bright magnitude limit, leaving a total of 871 objects.

2.2. The Homogeneous Bright QSO Survey

Data from the six deepest fields of the Homogeneous Bright QSO Survey (HBQS) were published by Cristiani et al. (1995) The six deepest fields of the HBQS contain either B_J or B' magnitudes for 285 QSOs in the range $15.5 < B_J < 18.85$, with faint magnitude limits ranging from 18.25 to 18.85. The bright magnitude limits are generally lower than those of the LBQS, varying from 14.0 to 16.0. For observations in the B_J band equation (4) was used and for observations in the B' band the equation

$$B = B' + 0.11(B - V) \quad (5)$$

of Blair and Gilmore (1982) was used assuming $B - V = 0.3$. Again, when combining this sample only objects in the redshift range $0.3 < z < 2.2$ were used, leaving a total of 254 objects.

2.3. The Durham/AAT Survey

The Durham/AAT survey contains 419 QSOs in the magnitude range $17 < b < 21.27$ (Boyle et al. 1990) and redshift range $0.3 < z < 2.2$, giving information about the QSO luminosity function in a different regime than the previous two samples. The faint magnitude limit ranges from 20.25 to 21.27 and the bright magnitude limit ranges from 16.4 to 18.0. The data are given in the “ b ” magnitude system, which according to Boyle et al. (1990) may be converted into the B system by the relation

$$B = b + 0.23(B - V - 0.9). \quad (6)$$

As above, the average value $B - V = 0.3$ was used to determine B .

2.4. The Edinburgh QSO Survey

A subsample of the Edinburgh QSO Survey (EQS) consisting of 12 QSOs brighter than $B = 16.5$ was published by Goldschmidt et al. in 1992. Of these, the 8 that fall in the redshift range $0.3 < z < 2.2$ were added to the combined samples to give information about the luminosity function at the bright end.

There have been several previous analyses of the above quasar surveys. Boyle et al. (1990) used binning techniques to fit the the Durham/AAT data to the PLE model. More recently, La

Franca and Cristiani (1996) fit the LBQS and HBQS data to a more complex luminosity function (involving 3 or more parameters) with no density evolution. Hatziminaoglou et al. (1998) examined the PLE and PDE cases separately using both the Durham/AAT and LBQS data. As described below, we combine all of these data and determine both the luminosity evolution $g(z)$ and the density evolution $\rho(z)$.

3. STATISTICAL METHODS

The statistical problem at hand is the determination of the true distribution of luminosities and redshifts of the sources from a biased or truncated data set, such as a flux limited sample. Several different techniques exist that give such a determination. The most common method is to bin the data and fit to some parametric forms of $\psi(L)$ or $\rho(z)$. However, it is preferable to avoid binning and to use non-parametric methods whenever possible. For a review of the various methods see Petrosian (1992). Assuming the general form of equation (3) for the luminosity function we must determine the functional forms of the local luminosity function $\psi(L_o, \alpha_i)$, density evolution $\rho(z)$ and the luminosity evolution $g(z)$ as well as the changes in the parameters α_i with redshift, if any. This last aspect is a higher order effect and will not be within the scope of this paper. We will discuss the certainty with which this can be ignored in the final analysis.

All non-parametric techniques for determining the distribution in a bivariate setting require that the data be expressed in terms of two uncorrelated variables, i.e. that we use variables x and y for which the density function is separable: $\Psi(x, y) = \rho(x)\psi(y)$. Thus before applying non-parametric methods one must first determine the degree of correlation of the data in the $x-y$ plane. This determination and the process of removing the correlation is equivalent to a determination of the functional form of the luminosity evolution $g(z)$ and the subsequent transformation $L \rightarrow L_o = L/g(z)$. This cannot be accomplished easily by non-parametric methods. Therefore, we chose two parametric forms for the luminosity evolution, $g_k(z)$ and $g_{k'}(z)$, and find the values of the parameters k and k' for which L_o and z are uncorrelated. Once this is done, the non-parametric methods described in Petrosian (1992) may be used to determine $\rho(z)$ and $\psi(L_o)$.

The methods normally used to test correlation and determine the distributions are suited for simple truncations, such as $y < f(x)$ (which by defining $x' = f(x)$ can be reduced to the generic case of $y < x'$). This is sufficient for simple flux limited data. However, the majority of astronomical data, and quasar data in particular, suffer from more than one truncation. The data may have an upper as well as a lower truncation, $f^-(x) < y < f^+(x)$, or there may be similar truncations in the value of the other variable. In addition, the functions $f^-(x)$ and $f^+(x)$ may not be continuous or even single valued. In general, multiply truncated redshift - magnitude data may be written as $\{z_i, m_i, [z_i^-, z_i^+], [m_i^-, m_i^+]\}_{i=1}^N$ where $[z_i^-, z_i^+]$ and $[m_i^-, m_i^+]$ are the observational limits on z and m for the i^{th} object, respectively. Given a cosmological model Ω this gives data of the form $\{z_i, L_i, [z_i^-, z_i^+], [L_i^-, L_i^+]\}_{i=1}^N$. If one assumes that each object has the same redshift limits $[z_i^-, z_i^+]$, which is the case in the majority of our analyses, then the problem is to test the

correlation and distribution of x and y from a data set $\{x_i, y_i\}_{i=1}^N$ given truncation limits $[y_i^-, y_i^+]$ for each point. The previous methods developed for this test (see Petrosian 1992 and Efron and Petrosian 1992) are suited for one sided truncations. In a more recent work (Efron and Petrosian 1998) we have developed methods, which are a generalization of the earlier methods, for dealing with doubly truncated data. We will briefly review these new methods of testing correlation and non-parametrically determining the density evolution and luminosity function.

3.1. Tests of Correlation and Determination of Luminosity Evolution

3.1.1. Untruncated data

If x and y are independent then the rank R_i of x_i in an untruncated sample (i.e. a sample truncated parallel to the x and y axes, so that y_i^\pm are independent of x_i) will be distributed uniformly between 1 and N with an expected mean $E = \frac{1}{2}(N + 1)$ and variance $V = \frac{1}{12}(N^2 - 1)$. One may then normalize R_i to have a mean of 0 and a variance of 1 by defining the statistic $T_i = (R_i - E)/V$. One then rejects or accepts the hypothesis of independence based on the distribution of the T_i .

One simple way of doing so is by defining a single statistic t_{data} based on the T_i with a mean of 0 and a variance of 1. One then rejects the hypothesis of independence if $|t_{data}|$ is too large (e.g. $|t_{data}| \geq 1$ for rejection of independence at the 1σ level). The quantity

$$\tau = \frac{\sum_i (R_i - E)}{\sqrt{\sum_i V}} \quad (7)$$

is one choice of such a test statistic. This τ is equivalent to Kendall's τ statistic, which is defined in the following manner. Consider all possible pairings $\mathcal{P} = \{(i, j)\}$ between data points and call a pairing (i, j) positive if $(x_i - x_j)(y_i - y_j) > 0$ and negative if $(x_i - x_j)(y_i - y_j) < 0$. If there are no ties then the τ of equation (7) is equivalent to Kendall's τ statistic

$$\tau = \frac{\# \text{ positive } (i, j) \in \mathcal{P} - \# \text{ negative } (i, j) \in \mathcal{P}}{\# (i, j) \in \mathcal{P}}. \quad (8)$$

3.1.2. Data with One-Sided Truncation

A straightforward application of this method to truncated data will clearly give a false correlation signal. Efron and Petrosian (1992), and independently Tsai (1990), describe how this method can be applied to data with one-sided truncation, i.e. either $y_i^- = -\infty$, $i = 1, \dots, N$ or $y_i^+ = \infty$, $i = 1, \dots, N$. For example, if $y_i^+ = \infty$ but y_i^- varies with x_i then the above procedure is modified as follows. For each object define the *comparable* or *associated* set

$$J_i = \{j : y_j > y_i, y_j^- < y_i\} \quad (9)$$

to consist of all objects of greater y for which the value $y = y_i$ could possibly be observed. This is the same set as defined in Lynden-Bell's C^- method and, unlike the definition of Efron and Petrosian (1992, e.g. (2.9)), does not include the object in question. In the case of luminosity-redshift data this is the largest subset of luminosity (not magnitude or flux) and volume limited data that can be constructed for each given (L_i, z_i) . If x and y are independent then we expect the rank R_i of x_i in the eligible set,

$$R_i = \#\{j \in J_i : x_j \leq x_i\}, \quad (10)$$

to be uniformly distributed between 1 and N_i , where N_i is the number of points in J_i . The rest of the procedure follows as for untruncated data. The normalized statistic T_i is defined here as $T_i = (R_i - E_i)/V_i$ where $E_i = \frac{1}{2}(N_i + 1)$ and $V_i = \frac{1}{12}(N_i^2 - 1)$. The test statistic τ is then defined by

$$\tau = \frac{\sum_i (R_i - E_i)}{\sqrt{\sum_i V_i}} \quad (11)$$

and is equivalent to a version of Kendall's τ statistic defined by equation (8). In this case, however, we consider only the set of possible pairings allowed by truncation $\mathcal{P} = \{(i, j) : y_i > y_j^-, y_j > y_i^-\}$.

3.1.3. Multiply Truncated Data

A generalization of the above method to doubly (or multiply) truncated data was developed recently by Efron and Petrosian (1998). The method is equivalent to the previous method, with the eligible set defined as

$$J_i = \{j : y_j > y_i, y_i \in (y_j^-, y_j^+)\} \quad (12)$$

and the set of allowed pairings

$$\mathcal{P} = \{(i, j) : y_i \in (y_j^-, y_j^+), y_j \in (y_i^-, y_i^+)\} \quad (13)$$

defined such that each object lies within the truncation region of the other.

In this case, however, the distribution of the rankings (or of τ) is unknown. If the data are uncorrelated then τ must still have a mean of zero and a bootstrap method may be used to determine the variance V_τ as follows. By assuming the data $\{x_i, y_i\}$ are uncorrelated one can use the methods of the next section to determine $\psi(y)$, the underlying (i.e. non-truncated) probability distribution of y . Once $\psi(y)$ is found one can simulate N_{sim} sets of data with underlying probability density $\psi(y)$ and truncation limits $[y_i^-, y_i^+]$ for the i^{th} object in each set. For each simulated set of data \mathcal{D}_k one may find τ_k as in equation (8) and estimate V_τ from the distribution of $\{\tau_k\}_{k=1}^{N_{sim}}$. For large numbers of simulations N_{sim} the error in this determination of V_τ is approximately $V_\tau/\sqrt{N_{sim}}$. Given V_τ one can define a normalized test statistic τ/V_τ with a mean of 0 and a variance of 1.

3.1.4. The Luminosity Evolution

If x and y , in this case the luminosity and redshift, prove to be independent, which would be the case if $|\tau| < 1$, one may assume that there is no luminosity evolution and proceed with the determination of the univariate distributions $\psi(L)$ and $\rho(z)$ of equation (1) using the methods described below. However, if $|\tau| \geq 1$ then L and z cannot be considered independent and one may assume that the most likely explanation is the presence of luminosity evolution ($g(z) \neq \text{constant}$). Another possibility is the variation of the shape parameters α_i with z . We will return to this possibility below. One can determine the function $g(z)$ parametrically as follows.

Given a parametric form for luminosity evolution $g_k(z)$ one can transform the luminosities into $L_o(k) = L/g_k(z)$ and proceed with the determination of the correlation $\tau(k)$ between L_o and z as a function of the parameter k . If τ is normalized to have a standard deviation of 1, then the values of k allowed by the data at the 1σ confidence level are $\{k : |\tau(k)| < 1\}$, and the most likely values of k are those with $\tau(k) = 0$. Although in principle it is possible for the function $\tau(k)$ to have several zeroes, this did not occur for the specific cases described in §5.

3.2. Non-Parametric Determination of Distribution Functions

Once a function g is found that removes the correlation between x and y (or z and L), the task is to find the underlying distributions $\rho(x)$ (the density evolution) and $\psi(y')$ (the local luminosity function) given uncorrelated data $\{x_i, y'_i = y_i/g(x_i)\}_{i=1}^N$ and truncation limits $[y'_i^-, y'_i^+]$. If the truncation is one-sided (e.g. $y'_i^+ = \infty$ for all i) then a variety of non-parametric methods can be used to determine the univariate distribution functions. As shown by Petrosian (1992) all non-parametric methods reduce to Lynden-Bell's (1971) method. As with the tests of correlation described above, the gist of this method is to find for each point the comparable set defined in equation (9) and the number N_i of points in this set. For example, the cumulative distribution in y' , $\Phi(y') = \int_{y'}^{\infty} \psi(t) dt$, is given by

$$\ln \Phi(y'_i) = \sum_{j < i} \ln\left(1 + \frac{1}{N_j}\right). \quad (14)$$

For doubly truncated data the comparable set is not completely observed, thus a simple analytic method such as the one described above is not possible. However, it turns out that a simple iterative procedure can lead to a maximum likelihood estimate of the distributions. Here we give a brief description of this method; for details the reader is referred to Efron and Petrosian (1998).

Assume that the underlying density function $\psi(y)$ is discretely distributed over the N observed values of y . If we let $\psi_i = \psi(y_i)$ be the probability density at y_i then $\Phi_i = \sum_j \psi_j$, where the summation includes all data points for which $y_j \in [y_i^-, y_i^+]$, is the total probability density for the

truncation region $[y_i^-, y_i^+]$. If we define the matrix \mathbf{J} by

$$J_{ij} = \begin{cases} 1, & \text{if } y_j \in [y_i^-, y_i^+] \\ 0, & \text{if } y_j \notin [y_i^-, y_i^+] \end{cases} \quad (15)$$

then the definition of Φ_i is equivalent to $\Phi = \mathbf{J} \cdot \Psi$ where $\Psi = (\psi_1, \dots, \psi_N)$ and $\Phi = (\Phi_1, \dots, \Phi_N)$. This matrix \mathbf{J} contains all of the information about the data and the truncation limits needed to find the vector of probability densities Ψ . We also have the normalization condition on Ψ ,

$$\sum_{i=1}^N \psi_i = 1. \quad (16)$$

From the definition of Φ it follows that the conditional probability $\psi(y_i | [y_j^-, y_j^+])$ of observing a value y_i within the truncation region $[y_j^-, y_j^+]$ is

$$\psi(y_i | [y_j^-, y_j^+]) = \begin{cases} \psi_i / \Phi_j, & \text{if } y_i \in [y_j^-, y_j^+] \\ 0, & \text{if } y_i \notin [y_j^-, y_j^+] \end{cases}. \quad (17)$$

The final condition on Ψ is determined by maximizing the likelihood of observing the actual data,

$$P_{data} = \prod_{i=1}^N \psi(y_i | [y_i^-, y_i^+]) = \prod_{i=1}^N \frac{\psi_i}{\sum_j J_{ij} \psi_j}. \quad (18)$$

By setting $\frac{\partial P_{data}}{\partial \Psi} = 0$ it follows that $\psi_k^{-1} = \sum_j J_{jk} \Phi_j^{-1}$, $k = 1, \dots, N$. This may be written compactly as

$$\frac{1}{\Psi} = \mathbf{J}^\dagger \frac{1}{\Phi} \quad (19)$$

with the notation $\frac{1}{\mathbf{a}} = (a_1^{-1}, \dots, a_N^{-1})$. Thus we have reduced the problem of finding the density function for data with arbitrary truncation to the “moral equivalent” of an eigenvalue problem for the matrix \mathbf{J} .

In practice, this condition may be used as a recursive formula to determine Ψ . One starts with an initial guess for the density vector Ψ^o . Equation (19) then gives the recursion relation

$$\frac{1}{\Psi^{(j+1)}} = \mathbf{J}^\dagger \frac{1}{\Phi^{(j)}} + c^{(j)} \quad (20)$$

where the constant $c^{(j)}$ is determined by the normalization condition $\sum_i \psi_i^{(j+1)} = 1$. One may use as an initial guess the untruncated solution $\psi_i^o = \frac{1}{N}$. In most problems, however, one of the two truncations will have a more pronounced effect than the other. In this case, one may ignore the weaker truncation and use the result based on the one-sided method as an initial guess. We found that with this initial guess and data confined to one region of the $L-z$ plane the sequence of $\Psi^{(j)}$ defined by equation (20) usually converged quickly. However, for combined samples spanning different regions of the $L-z$ plane it was helpful to use an algorithm to accelerate the convergence of the series of $\Psi^{(j)}$. For this purpose we used Aitken’s δ^2 method, which gives an improved estimate for the terms of series by assuming approximately geometric convergence (see, e.g. Press et al. 1992, chapter 5.1).

4. COSMOLOGY AND MODELS OF LUMINOSITY EVOLUTION

In order to determine the intrinsic parameters of an object from the observed data one must assume a certain cosmological model. Many cosmological models may be described in terms of a few fundamental parameters, which (see e.g. Peebles 1993) for a matter dominated (non-relativistic) universe are the matter density ρ_o , the cosmological constant Λ and the curvature of space k (which is +1, 0 or -1 for closed, flat or open universes, respectively). Using Hubble's constant H_o these parameters may be written in dimensionless form as

$$\Omega_M = \frac{8\pi G\rho}{3H_o^2}, \quad \Omega_k = -\frac{kc^2}{(H_o R_o)^2} \quad \text{and} \quad \Omega_\Lambda = \frac{\Lambda}{3H_o^2} \quad (21)$$

where R_o is the value of the expansion parameter of the universe at the present epoch. These three parameters are related via the Friedman-Lemaitre equation $\Omega_M + \Omega_k + \Omega_\Lambda = 1$, allowing us to eliminate one of them in favor of Hubble's constant. For example, the curvature term may be written

$$\Omega_k = 1 - (\Omega_M + \Omega_\Lambda). \quad (22)$$

We will consider the two classes of cosmological models given by $\Omega_\Lambda = 0$ (no cosmological constant) and $\Omega_k = 0$ (flat universe with cosmological constant). For calculations of the luminosity function we will pay particular attention to the two cases $\Omega_k = \Omega_\Lambda = 0$ and $\Omega_\Lambda = 0.85$, $\Omega_M = 0.15$. The first of these is the standard Einstein - de Sitter model, and the second is an inflationary model with parameters in accordance with current observations. For definiteness, Hubble's constant was assumed to be $H_o = 70$ km/(s Mpc), although most results are independent of this assumption.

Once the values of the cosmological parameters are fixed, calculations of intrinsic parameters are relatively straightforward (Peebles 1993). The absolute luminosity, for example, takes the form

$$L = f 4\pi d_L^2 K(z) \quad (23)$$

where f is the observed flux, the luminosity distance d_L is

$$d_L = \frac{c}{H_o} (1+z) \frac{\sin \sqrt{k} u(z)}{\sqrt{k}} \quad (24)$$

and $K(z)$ is the K-correction term. The co-moving coordinate distance is

$$u(z) = \int_0^z \frac{dz}{\sqrt{\Omega_M(1+z)^3 + \Omega_k(1+z)^2 + \Omega_\Lambda}} \quad (25)$$

and the co-moving volume contained within a sphere of radius corresponding to redshift z is

$$V(z) = 4\pi \left(\frac{c}{H_o}\right) \int_0^z \frac{du}{dz} \frac{d_L^2}{(1+z)^2} dz. \quad (26)$$

In general, these integrals must be evaluated numerically.

In order to determine the K-correction term $K(z)$ one must make an assumption about the quasar spectrum in the optical region. The general practice here is to assume a power law spectrum $L_{optical} \propto \nu^\alpha$ with spectral index $\alpha \simeq -0.5$, which gives $K(z) = (1+z)^{1+\alpha} \simeq \sqrt{1+z}$.

Two models for luminosity evolution were used: $g_k(z) \propto e^{kt(z)}$ and $g_k(z) \propto (1+z)^k$. The first of these assumes an exponential dependence on the fractional lookback time $t(z)$, which is defined as $t(z) = 1 - T(z)/T(0)$, where $T(z)$ is the age of the universe at redshift z ,

$$T(z) = H_o^{-1} \int_z^\infty \frac{du}{dz} \frac{dz}{(1+z)}. \quad (27)$$

The second model assumes a power law dependence on the scale factor of the universe (or the expansion parameter R), which is independent of the cosmological parameters. Analyses of earlier data (see e.g. Caditz and Petrosian 1990) have traditionally given estimates of quasar evolution for these two parametric forms of $g(z) \approx e^{7.5t(z)}$ and $g(z) \approx (1+z)^3$.

5. THE EVOLUTION OF THE LUMINOSITY FUNCTION

In what follows we apply the procedures of §3 to determine the correlation between the luminosities and redshifts and test parametric forms for the evolution of the luminosity, the function $g(z)$. Then we transform all luminosities to their present epoch values $L_o = L/g(z)$ and determine the co-moving density evolution $\rho(z)$ and the present epoch luminosity function $\psi(L_o)$ for the cosmological models described in §4. We apply these tests to the surveys described in §2 individually and in various combinations. Before presenting these results we discuss briefly the redshift - magnitude data, i.e. the Hubble diagram shown in Figure 1.

5.1. The Quasar Hubble Diagram

As is evident from Figure 1, at first glance there seems to be very little correlation between the redshifts and magnitudes (or fluxes) of quasars; i.e. there is no obvious evidence for a Hubble type relation. This result is well known. For example, a preliminary test of correlation between m and z in a small subsample by Efron and Petrosian (1992, Figure 6) showed no correlation. Earlier, the absence of a clear Hubble relation was used as an argument against the cosmological origin of quasar redshift (see, e.g. Burbidge and O'Dell 1973). This is not the only possible interpretation, however. One would not expect a simple Hubble diagram for sources with a broad luminosity function (non-standard candle sources, see e.g. Petrosian 1974). The absence of an obvious Hubble relation can also arise from approximate cancelation between cosmological dimming and luminosity evolution. Exact cancelation of these two effects is highly implausible and could bring into question the basic assumptions about the distribution of sources. To clarify this situation we have applied the correlation tests described in §3 to the surveys of §2. First ignoring the high flux (low magnitude)

limit, i.e. with $m_{min} = -\infty$, we use the one-sided tests and find the results labeled τ_1 shown in Table 1. When using the double-sided tests we find the results τ_2 , which indicate slightly less correlation, as expected because the one-sided methods ignore the slight truncation induced by the high flux limits. These tests, when applied to the combined data sets, give a correlation of $\tau = 3.63$. This result rejects the hypothesis of independence between B and z at the 99.97% confidence level and is independent of any cosmological parameters. In addition, we may test the parametric fit $B(z) = B - \beta \log(d_L^2(z, \Omega)K(z)) + \text{constant}$ for the data using the methods for multiple truncations to determine the best value of β , i.e. the value for which $B(z)$ and z are uncorrelated ($\tau = 0$). A value of $\beta = 2.5$ is what one would expect for standard candle sources with a very narrow luminosity function, while a value of $\beta = 0$ would mean the complete absence of a Hubble relation and the exact cancelation described above. The results shown in Table 1 indicate that β , while clearly less than 2.5, differs significantly from 0 for the cosmological models discussed in §4. The best parametric fit for the Einstein - de Sitter cosmological model ($\beta = 0.84$) is shown in Figure 1 along with the expected relation for standard candle sources ($\beta = 2.5$).

We now turn to a determination of the evolution of the luminosity.

5.2. The Luminosity Evolution $g(z)$

We examine the two commonly used parametric forms for the luminosity evolution, the exponential and power law forms. These two different forms emphasize the evolution in different regions of the luminosity - redshift ($L - z$) plane. A correct parameterization will have the same value for its parameters when applied to samples with different limits (i.e. different coverage of the $L - z$ plane). This fact can be used to test a given parametric form. Table 2 summarizes the results described in the subsequent sections. Figure 2 gives an example of the variation of the test statistic τ as a function of the evolution parameter k . The optimal value of k , i.e. the value which indicates that L_o and z are not correlated, is given by the condition $\tau = 0$ and the 1σ range of this parameter is given by the condition $|\tau| < 1$. These values are shown in Figure 2.

5.2.1. Evolution of the form $g_k(z) \propto e^{kt(z)}$

Figures 3a and 3b display the best values and the 1σ ranges for the evolution parameter k assuming both $\Omega_\Lambda = 0$ and $\Omega_k = 0$ cosmological models for the different samples. The Durham/AAT data exhibit much stronger evolution than the other data, indicating that this form of evolution does not adequately describe the data in the entire $L - z$ plane. The values of k found for most of the data sets are considerably less than the previously determined value $k \approx 7.5$ by Caditz and Petrosian (1990), which was dominated by the Durham/AAT data.

5.2.2. Evolution of the form $g_{k'}(z) \propto (1 + z)^{k'}$

| Sample | N | τ_1 | P_1 | τ_2 | P_2 | β_1 | β_2 |
|---------------|------|----------|-------|----------|-------|-----------|-----------|
| Durham/AAT | 419 | -0.65 | 48.71 | -0.45 | 35.02 | -0.22 | -0.18 |
| LBQS | 871 | 4.65 | 99.99 | 3.75 | 99.98 | 1.11 | 0.92 |
| HBQS | 254 | 1.37 | 82.92 | 1.27 | 79.42 | 0.71 | 0.59 |
| LBQS and HBQS | 1125 | 4.80 | 99.99 | 3.98 | 99.99 | 1.01 | 0.83 |
| Combined Data | 1552 | 3.98 | 99.99 | 3.63 | 99.97 | 0.84 | 0.70 |

Table 1: Correlation data for the Quasar Hubble Diagram. N is the number of data points in each of the data sets of §2. The correlation τ and the probability value P for rejection of independence between B magnitude and redshift z are given. The first set of values (τ_1 , P_1) are found using the one-sided method of Efron and Petrosian (1992) and the second set of values (τ_2 , P_2) are found using the general method for doubly truncated data presented in §3. The parameters β_1 and β_2 are found with this general method by fitting to the equation $B(z) = B - \beta \log(d_L^2(z)K(z)) + \text{constant}$ for the two cosmological models $\Omega_M = 1$, $\Omega_\Lambda = 0$ and $\Omega_M = 0.15$, $\Omega_\Lambda = 0.85$ respectively.

| Sample | N | k | k_{min} | k_{max} | k' | k'_{min} | k'_{max} |
|---------------|------|------|-----------|-----------|------|------------|------------|
| Durham/AAT | 419 | 8.72 | 6.66 | 10.07 | 3.53 | 2.57 | 5.05 |
| HBQS | 254 | 5.39 | $-\infty$ | 6.49 | 3.20 | $-\infty$ | 3.94 |
| LBQS | 871 | 4.28 | 2.66 | 5.17 | 2.02 | 1.24 | 2.53 |
| Combined Data | 1552 | 5.15 | 4.36 | 5.70 | 2.58 | 2.14 | 2.91 |

Table 2: Values of the evolution parameters k and k' for the different data sets. These parameters refer to luminosity evolutions $g_k(z) \propto e^{kt(z)}$ and $g_{k'}(z) \propto (1+z)^{k'}$, respectively. The minimum and maximum values are those allowed at the 1σ level. Note the variation in k and the near constancy of k' .

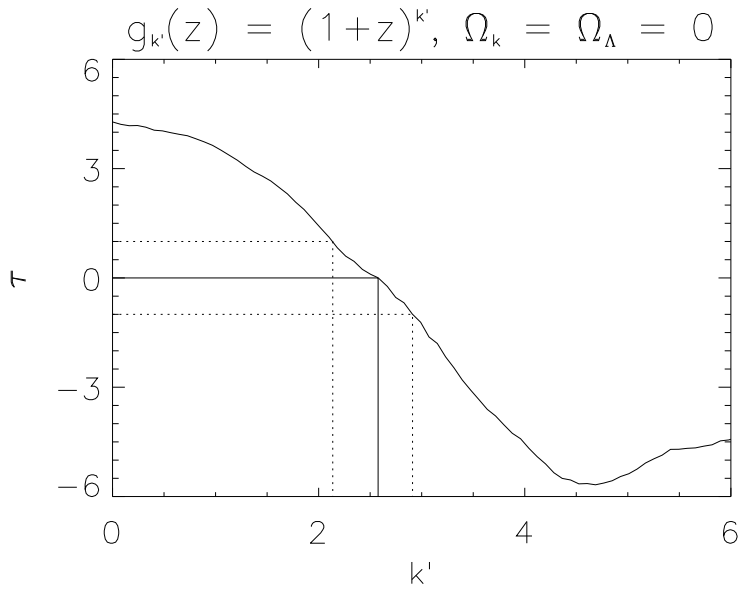


Fig. 2.— A determination of the luminosity evolution parameter for the parametric form $g_{k'}(z) \propto (1+z)^{k'}$. The correlation statistic τ is shown as a function of k' for the combined data set for the Einstein - de Sitter cosmological model. We use the correlation test for multiply truncated data of §3, normalized so that τ has a standard deviation of 1. The solid line at $\tau = 0$ demonstrates the determination of the optimal value $k' = 2.58$ and the dashed lines at $|\tau| = 1$ demonstrate the determination of the 1σ region $[2.14, 2.91]$.

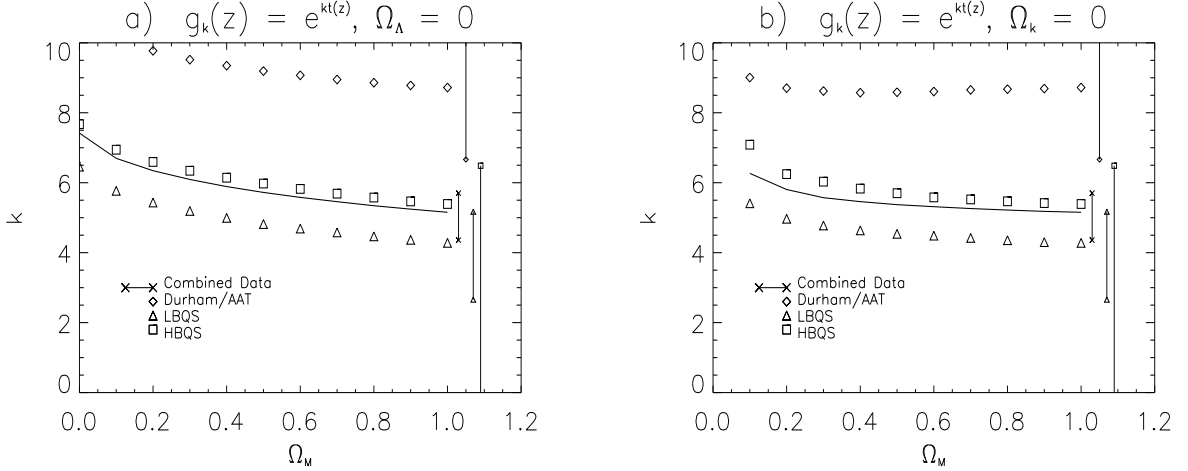


Fig. 3.— Variation of the evolution parameter k with Ω_M for evolution of the form $g_k(z) \propto e^{kt(z)}$ for the three major surveys and for the combined data set. One σ error bars are plotted for the $\Omega_M = 1$ case. Error bars are similar for the other values of Ω_M . Note the significant difference between the deeper Durham/AAT data and the LBQS and HBQS data. This may indicate that the choice of $g_k(z)$ is not correct. Figure a) shows results for cosmological models with $\Omega_\Lambda = 0$ and $\Omega_k = 1 - \Omega_M$. Figure b) shows results for cosmological models with $\Omega_k = 0$ and $\Omega_\Lambda = 1 - \Omega_M$.

Figures 4a and 4b give results for the evolution parameter k' for the same cosmological models as above. The allowed ranges obtained from the different samples are much closer, thus this form of evolution is shown to be a closer approximation to the actual evolution than the exponential form. For the Einstein - de Sitter model, the best value of evolution parameter is $k' = 2.58$ with a one σ range of $k' \in [2.14, 2.91]$. As with the previous case, the values of k' are somewhat less than the previously found value of $k' \approx 3$ of Caditz and Petrosian (1990).

It is clear that a better fit can be achieved with a different functional form for $g(z)$ with two or more parameters. However, in what follows we assume the simpler form of evolution $g(z) \propto (1+z)^{k'}$ with $k'(\Omega)$ the optimal value of k' for a given cosmological model Ω . We therefore transform the data to $\{[L_{oi}, z_i]\}_{i=1}^N$ with $L_o(z, m, \Omega) = L(z, m, \Omega)/(1+z)^{k'}$ and apply the method of §3 to find non-parametric estimates for the density functions $\rho(z)$ and $\psi(L_o)$. This method now gives directly the cumulative functions $\sigma(z) = \int_0^z \rho(z) \frac{dz}{dz} dz$ and $\Phi(L_o) = \int_{L'}^\infty \psi(L') dL'$.

5.3. The Density Evolution $\rho(z)$

The cumulative density function $\sigma(z)$ is the total number of objects within the angular area of the survey up to redshift z . If there is no density evolution, i.e. $\rho(z) = \rho_o$ is a constant, then $\sigma \propto V$ where $V(z)$ is the co-moving volume up to redshift z . We determine $\sigma(z)$ and $\rho(z)$ using the new

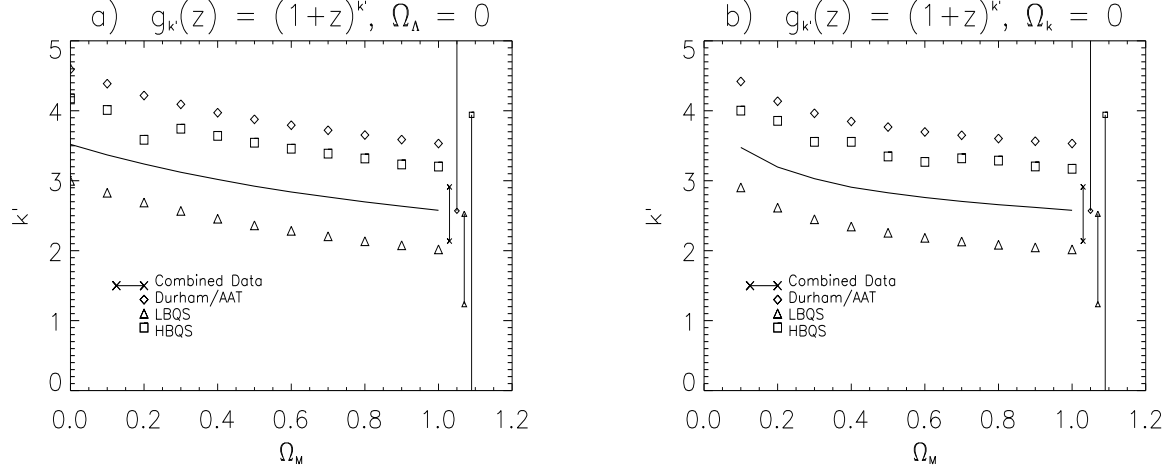


Fig. 4.— Same as Figure 3 with evolution of the form $g_{k'}(z) \propto (1+z)^{k'}$. The error bars nearly overlap at the optimal value for the combined data, indicating that this is a better parameterization over the observed range of the $L - z$ plane.

method for doubly truncated data. In order to determine if density evolution exists we fit σ to V by a simple power law $\sigma(z) \propto V^\lambda$, where $\lambda \neq 1$ indicates the presence of density evolution. If the density increases with redshift we expect $\lambda > 1$ and if the density decreases with redshift we expect $\lambda < 1$. Even if $\lambda = 1$, however, density evolution may be present: the density may increase and decrease in such a way as to cancel and give a fit of $\lambda = 1$. Figures 5a and 5b show the variation of σ and ρ with V for the combined sample for three different cosmological models. The dotted lines show the best fits to the form $\sigma \propto [V(z, \Omega)]^\lambda$. For the Einstein - de Sitter model (top curves in Figure 5) we have $\lambda = 1.19$, indicating that the co-moving density increases with redshift roughly as $\sigma \propto V^{1.19}$. This would indicate a simple power law density evolution $\rho \propto V^{0.19}$. The density evolution shown in Figure 5b exhibits this average behavior, but in detail is more complex: the density increases more rapidly at low z , reaches a plateau at $z \approx 2$ and possibly decreases at higher z . This behavior will be discussed below in more detail and for higher redshift data.

As mentioned in §1, one cannot determine the evolution of sources (the function $\rho(z)$) and the evolution of the universe (the parameters Ω_i) simultaneously. Given one of these (e.g. the cosmological model), the other (the density evolution) may be determined from the data. The variation of $\lambda = d \ln \sigma / d \ln V$ with Ω_M for the two different classes of cosmological models is shown in Figures 6a and 6b. It is evident that there is a monotonic variation of λ with Ω_M . In particular, $\lambda = 1$ for the two cosmological models: $\Omega_M \approx 0$, $\Omega_\Lambda \approx 1$ and $\Omega_M \approx 0.15$, $\Omega_\Lambda \approx 0.85$. This second set of parameters is quite close to those currently favored by many observations. As above, this does not imply the complete absence of density evolution. The lower two curves in Figure 5b show the variation of ρ for these two models. Clearly, there is less variation than for the Einstein - de Sitter model, but the general behavior is similar.

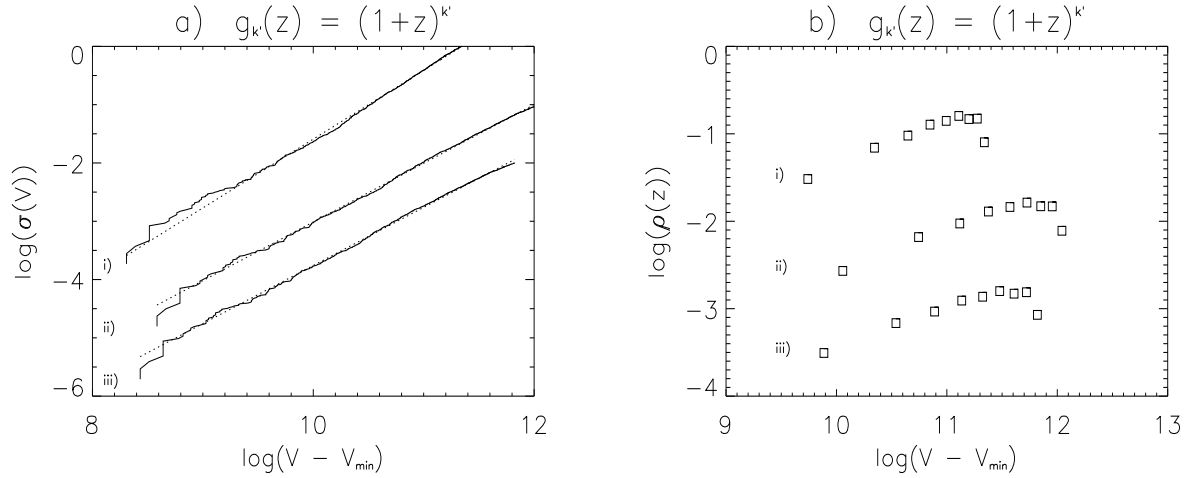


Fig. 5.— A plot of a) $\sigma = \int_0^z \rho(z') dz'$ and b) ρ as a function of co-moving volume $V(z, \Omega)$ for the combined data set for three different cosmological models. Curves i), ii) and iii) show results for Einstein - de Sitter, $\Omega_M = 0.15$, $\Omega_\Lambda = 0.85$ and $\Omega_M = 0$, $\Omega_\Lambda = 0$ models, respectively. Vertical normalizations are arbitrary. The straight dotted lines show the best fits to the parametric models $\sigma \propto V^\lambda$, with $\lambda = 1.19$ for the Einstein - de Sitter model and $\lambda = 1$ for the other two models. It is clear from b), however, that the model $\sigma \propto V^\lambda$ is only a rough approximation. In fact, ρ undergoes more complicated evolution, increasing and peaking before decreasing at higher redshift. The luminosity evolution $g_{k'}(z) \propto (1+z)^{k'}$, with the optimal value of $k' = 2.58$, was used to remove the correlation from the original data.

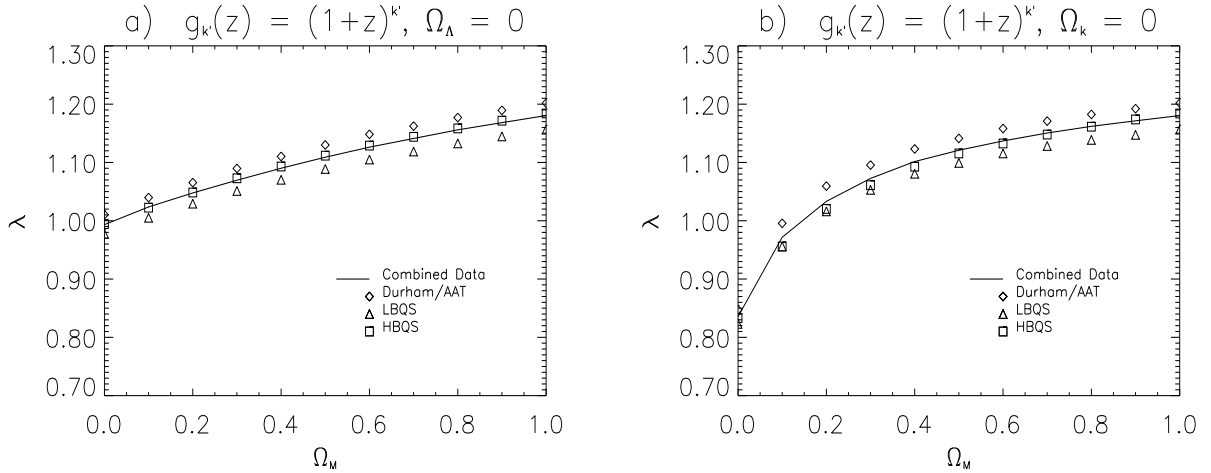


Fig. 6.— The best fit for the power law index $\lambda = d \ln \sigma / d \ln V$ is shown as a function of Ω_M for two different types of cosmological models. The index λ is defined by the equation $\sigma(z) \propto V^\lambda$, where $V(z, \Omega)$ is the co-moving volume of space contained within the sphere of radius $R(z)$. A value of $\lambda < 1$ corresponds to a decrease in density with redshift and $\lambda > 1$ corresponds to an increase in density with redshift. Pure luminosity evolution, $\lambda = 1$, ($\sigma \propto V(z)$) occurs for models without cosmological constant at $\Omega_M \approx \Omega_\Lambda \approx 0$ and for models without curvature at $\Omega_M \approx 0.15, \Omega_\Lambda \approx 0.85$. Figure a) shows results for cosmological models with $\Omega_\Lambda = 0$. Figure b) shows results for models with $\Omega_k = 0$.

To further analyze the variation of $\rho(z)$, in Figure 7 we show our non-parametric determination of $\rho(z)$ for the Einstein - de Sitter cosmological model. Two sets of results are given. The first of these (depicted by squares) shows $\rho(z)$ in the region $0.3 < z < 2.2$ from the combined data. The second (triangles) shows $\rho(z)$ in the region $0.3 < z < 3.3$ from the LBQS data (which do not have a high redshift cutoff at $z = 2.2$) alone. As evident in Figure 7, the density increases relatively slowly at low redshift ($\rho \sim (1+z)^{2.5}$) before reaching a peak at $z \approx 2$ and decreasing rapidly ($\rho \sim (1+z)^{-5}$) at higher redshift. As discussed further in §5.5, the decrease in density present in this data at redshift of about 2 is in agreement with high redshift survey results (Schmidt et al. 1995, Warren et al. 1994).

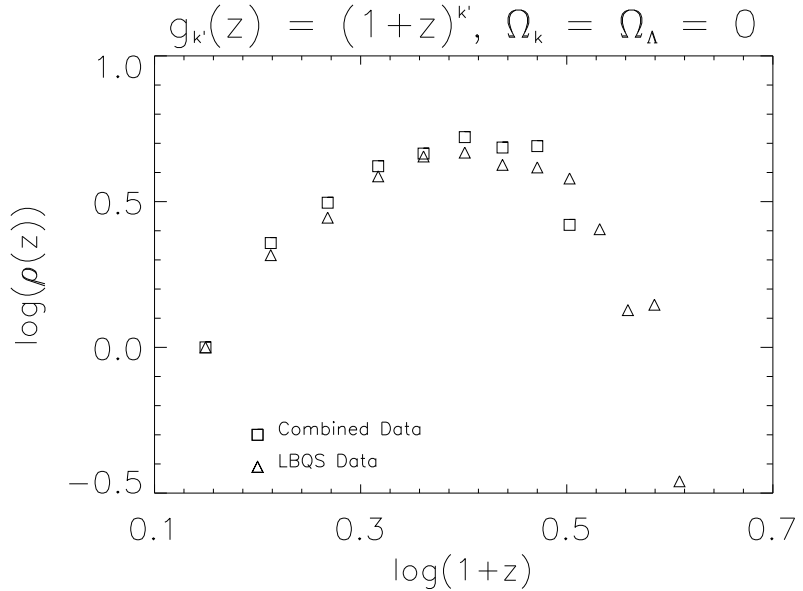


Fig. 7.— The non-parametric results for the density function $\rho(z)$ for the Einstein - de Sitter cosmological model. Clearly, a simple model $\rho \propto (1+z)^\mu$ will not adequately describe the density evolution. The squares show the results for the combined data in the region $0.3 < z < 2.2$ and the triangles show the results for the LBQS data in the region $0.3 < z < 3.3$. The density peaks at $z \approx 2$.

5.4. The Luminosity Function $\psi(L_o)$

In a similar fashion we may obtain the cumulative luminosity function $\Phi(L_o)$ from the uncorrelated data set $\{L_o, z\}$. Figures 8a and 8b show $\Phi(L_o)$ for the combined data set with $k' = 2.58$, along with the best fits to a double power law form

$$\Phi(L_o) = \frac{\Phi_o}{(L_o/L_*)^{k_1} + (L_o/L_*)^{k_2}}. \quad (28)$$

We used the cosmological models $\Omega_M = 1$, $\Omega_\Lambda = 0$ (Einstein - de Sitter model) and $\Omega_M = 0.15$, $\Omega_\Lambda = 0.85$ (pure luminosity evolution with cosmological constant). In both cases, the results for the combined samples exhibit roughly double power law dependence on L_o with similar values of the fitting parameters. The primary differences between the two models are that the Einstein - de Sitter model gives a slightly gentler slope above the break luminosity, $k_2 = 3.17$ as opposed to $k_2 = 3.59$, and a lower break luminosity, $L_* = 6.19 \times 10^{29}$ erg / (sec Hz) as opposed to $L_* = 9.48 \times 10^{29}$ erg / (sec Hz).

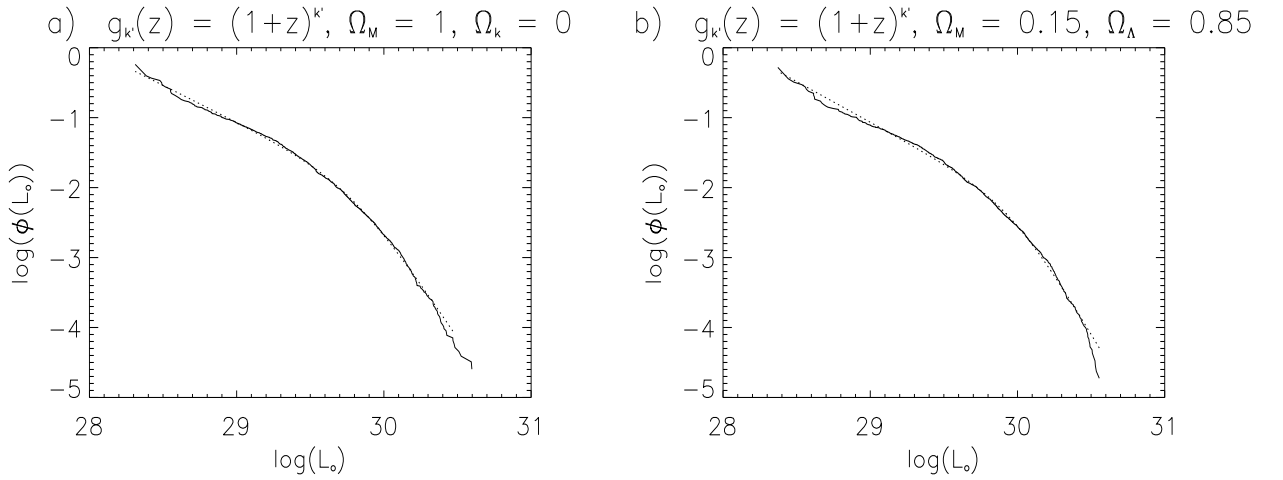


Fig. 8.— The cumulative luminosity function $\Phi(L_o) = \int_{L_o}^{\infty} \psi(L') dL'$ for the combined data set is shown as a function of $L_o = L/(1+z)^k$ for two different cosmological models. The dotted curve is the best fit to a double power law model, equation (28). Figure a) shows results for the Einstein - de Sitter model. In this case, the best fit to the double power law form has break luminosity $L_* = 6.19 \times 10^{29}$ erg / (sec Hz) and power law indices $k_1 = 1.05$ and $k_2 = 3.17$. Figure b) shows results for a cosmological model with $\Omega_M = 0.15$ and $\Omega_\Lambda = 0.85$. The best fit for this model has break luminosity $L_* = 9.48 \times 10^{29}$ erg / (sec Hz) and power law indices $k_1 = 1.16$ and $k_2 = 3.59$.

We check for possible variation in the shape of $\psi(L_o)$ by dividing the data into three redshift bins: $0.3 < z < 0.86$, $0.86 < z < 1.48$, and $1.48 < z < 2.2$. We then find the differential luminosity function $\psi(L_o)$ for these three redshift bins, first assuming no luminosity evolution ($g(z) = \text{constant}$) and then assuming luminosity evolution $g(z) \propto (1+z)^{k'}$. These luminosity functions (with arbitrary vertical normalization) are shown in Figures 9a and 9b, respectively. The presence of a strong shift to higher luminosities is clearly evident for $g(z) = \text{constant}$. However, when the evolution $g(z) \propto (1+z)^{k'}$ is taken out the luminosity function seems to exhibit little variation; the slopes appear roughly the same at low L_o and high L_o and the break luminosity does not vary as much with redshift. Although imprecise, these results indicate that our choice of $g(z)$ removes most of the variation of the parameters α_i with redshift, i.e. the shape of the luminosity function is almost invariant.

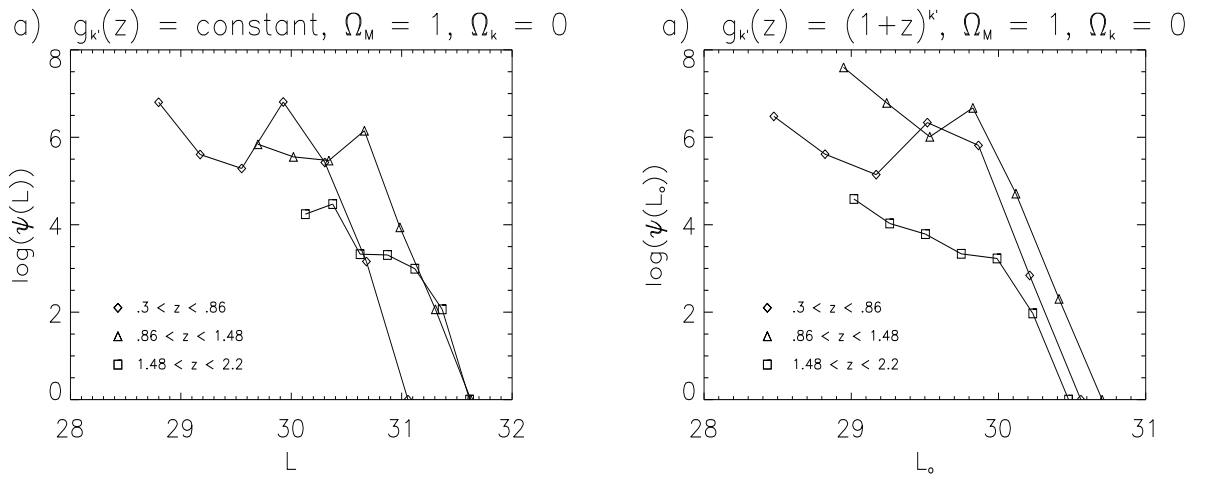


Fig. 9.— The luminosity function $\psi(L_o)$ for three different redshift bins (containing equal numbers of sources) for the Einstein - de Sitter cosmological model. Vertical normalization is arbitrary. Figure a) shows results assuming no luminosity evolution, $g(z) = \text{constant}$. Figure b) shows results assuming luminosity evolution $g(z) \propto (1+z)^{k'}$ with the optimal value of the parameter $k' = 2.58$ found above. The second figure shows small variation in the shape of $\psi(L_o)$ with redshift, indicating that most of the variation of the parameters α_i is removed by the choice of luminosity evolution $g(z) \propto (1+z)^{k'}$. As expected, the high luminosity end can be fitted to a power law with index $k_2 + 1 \simeq 4$.

5.5. The Luminosity Density $\mathcal{L}(z)$

Finally, we determine the luminosity density function $\mathcal{L}(z)$. This quantity is defined as the total rate of energy production by quasars in the optical range as a function of redshift; $\mathcal{L}(z) = \int_0^\infty L\psi(L)dL$. If the shape of the luminosity function is invariant then $\mathcal{L}(z) \propto \rho(z)g(z)$. This rate depends in a complicated way on the distribution of masses of the central black holes and the variation of the accretion rate, both of which are related to the formation of galaxies and their evolution through mergers or collisions. Using the above results we can evaluate $\mathcal{L}(z)$ up to a redshift of 2.2. We extend this further to a redshift of 3.3 using the LBQS data, which is claimed to be complete up to this redshift. These results, with arbitrary vertical normalization, are shown in Figure 10. We first note the good agreement in the $z < 2$ region, indicating that perhaps the LBQS result at higher redshift is a representative behavior. We may also use high redshift surveys of quasars (Schmidt et al. 1995, Warren et al. 1994) to study $\mathcal{L}(z)$ in this range. Unfortunately, the selection of high z quasars in these samples is more complicated and the subsequent analyses involve more assumptions. For example, Schmidt et al. use the V/V_{max} method to determine $\rho(z)$, tacitly assuming that $g(z) = \text{constant}$ (as well as $\alpha_i = \text{constant}$) so that $\mathcal{L}(z) \propto \rho(z)$. We show these results (again with arbitrary vertical normalization) in Figure 10. These results agree with the general trend of decline in $\mathcal{L}(z)$ at high redshifts.

It has been claimed (Cavaliere and Vittorini 1998, Shaver et al. 1998) that this rise and fall of $\mathcal{L}(z)$ with redshift is similar to the behavior of the star formation rate (SFR), which has recently been extended to high redshift (see, e.g. Madau 1997). We have shown this rate in Figure 10 as well. Although the general trend of rise and fall of the SFR and $\mathcal{L}(z)$ is the same, there is considerable difference in the detailed variation. The similarity may indicate some relation between the SFR and the feeding of the central engine of the quasars (e.g. both are affected by mergers). However, considering the many differences between star formation and the generation of energy by quasars, the observed difference between the SFR and $\mathcal{L}(z)$ in Figure 10 is not surprising.

6. SUMMARY AND CONCLUSIONS

Although there have been several analyses of quasar evolution in the past, our results differ from these previous results in two important respects:

- We have used non-parametric statistical methods for multiply truncated data that allow us to combine samples with different selection criteria.
- We have used the data to study models of the luminosity function that take into account both luminosity evolution $g(z)$ and density evolution $\rho(z)$.

The new non-parametric statistical methods differ from those used in the past in the following ways:

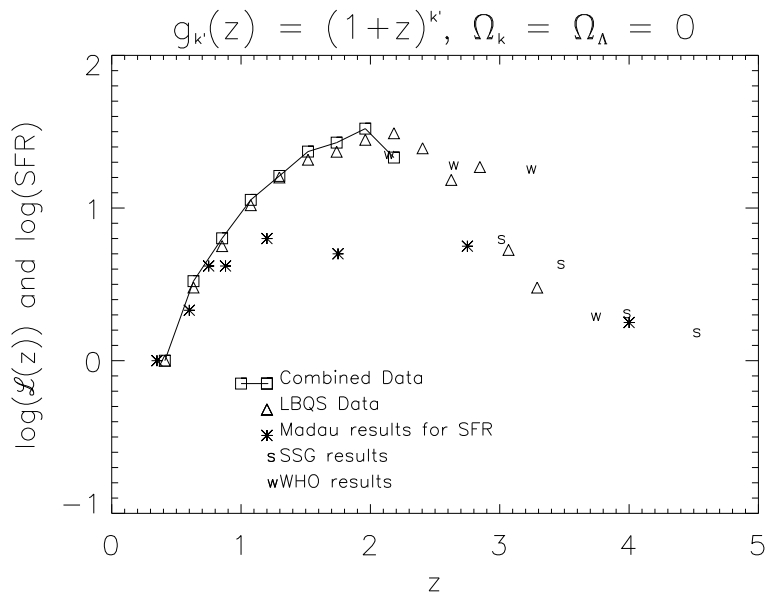


Fig. 10.— The luminosity density $\mathcal{L}(z)$ is shown as a function of redshift for the Einstein - de Sitter cosmological model. The squares and triangles give our results for the combined data and the LBQS data, respectively. The high redshift results of Schmidt et al. (1995) and Warren et al. (1994) are given by the letters “s” and “w”, respectively. The vertical normalizations are arbitrary. All of the above results indicate that \mathcal{L} peaks somewhere in the region $z \approx 2$. The stellar formation rate (SFR) as a function of redshift, as found by Madau (1997), is given by the asterisks. Although the SFR also exhibits the same general behavior as $\mathcal{L}(z)$, the peak occurs at a lower redshift and appears somewhat broader.

- No binning is required and most of the characteristics of the distribution functions are determined non-parametrically.
- The methods are not limited to simply truncated data such as that found in flux limited surveys and can account for selection biases in generally truncated data where each data point has different truncation limits. In particular, these methods can treat samples with both upper and lower flux limits and redshift limits.
- This versatility allows one to combine data from different surveys with different selection criteria.
- The first of our techniques, a generalized non-parametric test of independence, allows one to determine the degree of correlation between luminosity and redshift, giving an indication of the luminosity evolution in the luminosity function. The evolution may then be determined parametrically.
- The second of our techniques provides a non-parametric estimate for the univariate distributions in redshift and luminosity, i.e. the co-moving density evolution and the local luminosity function, respectively.

We have applied these methods to the combined data from several large surveys and determined the luminosity evolution $g(z)$, the density evolution $\rho(z)$ and the luminosity function $\psi(L_o = L/g(z))$ of the generalized luminosity function of equation (3) for flat ($\Omega_k = 0$ and $\Omega_M = 1 - \Omega_\Lambda$) and zero cosmological constant ($\Omega_\Lambda = 0$ and $\Omega_M = 1 - \Omega_k$) cosmological models. We assume a shape invariant luminosity function, $\alpha_i = \text{constant}$. More complex luminosity functions, $\alpha_i \neq \text{constant}$, or those with luminosity dependent density evolution, etc., can be tested if the simpler prescription used here is not consistent with all of the data. We found that the scenario of equation (3) provides an adequate description of the existing data.

Our results may be summarized as follows:

- We found a strong correlation between luminosity and redshift, indicating the presence of rapid luminosity evolution.
- The parametric model of luminosity evolution $(1 + z)^{k'}$ provides a better description of the data than the model $e^{kt(z)}$, although neither parameterization perfectly removes the correlation in all areas of the $L - z$ plane. In order to better model this evolution future analyses of quasar evolution could consider other parametric forms, including those with more than one free parameter.
- The cumulative co-moving density of quasars may be approximately modeled as $\sigma(z) \propto V^\lambda$, where the value of λ depends on the cosmological model. For example, $\lambda = 1.19$ for the Einstein - de Sitter model and $\lambda = 1$ for the cosmological models with $\Omega_M \approx 0$, $\Omega_k \approx 1$ and $\Omega_M \approx 0.15$, $\Omega_\Lambda \approx 0.85$. This simple parameterization $\sigma \propto V^\lambda$ does not describe precisely the variation of ρ with redshift. When examined in greater detail, the co-moving density shows a relatively slow increase ($\rho \sim (1 + z)^{2.5}$) for low redshifts and a rapid decline ($\rho \sim (1 + z)^{-5}$) for $z > 2$ (for the Einstein

- de Sitter model). This is in qualitative agreement with the observed density evolution of high z quasars (Schmidt et al. 1995, Warren et al. 1994). Qualitatively similar behavior is found even for models that show no overall density evolution ($\lambda = 1$). A more rigorous comparison cannot be made at this stage because the analysis of the high z data ignores possible $L - z$ correlation and assumes pure density evolution.

- The cumulative local luminosity function $\Phi(L_o) = \int_{L_o}^{\infty} \psi(x)dx$ has a double power law form. In the Einstein - de Sitter model the break luminosity is $L_* = 6 \times 10^{29}$ erg / (sec Hz) and the low and high luminosity power law indices are $k_1 = 1.05$ and $k_2 = 3.17$. There appears to be little variation with redshift of the shape of the cumulative and differential luminosity functions, thus the $\alpha_i = \text{constant}$ prescription seems adequate. With more data one could determine precisely the variation with redshift of the shape of $\phi(L_o)$.
- The above description of the luminosity function allows us to determine the rate of energy generation per unit co-moving volume of quasars as a function of redshift. We show that this function $\mathcal{L}(z) \propto \rho(z)g(z)$ increases rapidly with z at low redshift, peaks around $z \approx 2$ and then decreases. This is also in rough agreement with the high z survey results mentioned above. This variation of $\mathcal{L}(z)$ is similar to but significantly different from recent determinations of the star formation rate.

We would like to thank Bradley Efron for his invaluable help with the statistical methods used in this paper, Paul Hewett for help with the analysis of the LBQS data and Nicole Lloyd for helpful discussions. A. M. would like to acknowledge support from the Stanford University Undergraduate Research Opportunity program.

REFERENCES

Blair, M., and Gilmore, G. 1982, P.A.S.P., 94, 742.

Boyle, B. J., Fong, R., Shanks, T., and Peterson, B. A. 1990, M.N.R.A.S., 243, 1.

Burbidge, G. R., and O'Dell, S.L. 1973, Ap.J., 183, 759.

Caditz, D., and Petrosian, V. 1990, Ap.J., 357, 326.

Caditz, D., Petrosian, V., and Wandel, A. 1991, Ap. J. (Letters), 372, L63.

Cavaliere, A., and Padovani, P. 1988, Ap.J. (Letters), 333, L33.

Cavaliere, A., and Vittorini, V. 1998, to appear in *The Young Universe*, Eds. S. D'Odorico, A. Fontana and E. Giallongo ASP Conf. Series 1998. astro-ph/9802320 v2.

Cristiani, S., La Franca, F., and Andreani, P., et al. 1995, A. & A.S., 112, 347.

Efron, B., and Petrosian, V. 1992, Ap.J., 399, 345.

Efron, B., and Petrosian, V. 1998, JASA, in press.

Giaconi, R., et al. 1979, Ap.J.(Letters), 234, L1.

Goldschmidt, P., Miller, L., La France, F., and Cristiani, S. 1992, M.N.R.A.S., 256, 65.

Hawkins, M. R. S., and Véron, P. 1996, M.N.R.A.S., 281, 348.

Hatziminaoglou, E., Van Waerbeke, L. and Mathez, G. 1998, A & A, in press. astro-ph/9802267 v3.

Hewett, P. C., Foltz, C. B., and Chaffee, F. H. 1995, A.J., 109, 1498.

Koo, D. C., and Kron, R. G. 1988, Ap.J., 325, 92.

La Franca, F., and Cristiani, S. 1996, invited talk in *Wide Field Spectroscopy* (20-24 May 1996, Athens), Eds. M. Kontizas et al. astro-ph/9610017.

Lynden-Bell, D. 1971, M.N.R.A.S., 155, 95.

Lynds, R. C., and Wills, D. 1972, Ap.J., 175, 531.

Madau, P. 1997, to appear in *The Hubble Deep Field*, Eds. M. Livio, S. M. Fall, and P. Madau, STScI Symposium Series. astro-ph/9709147.

Marshall, H. L. 1985, Ap.J., 299, 109.

Peebles, P.J.E. 1993, *Principles of Physical Cosmology*, (Princeton, New Jersey : Princeton University Press).

Petrosian, V. 1974, Ap.J., 188, 443.

Petrosian, V. 1973, Ap.J., 183, 359.

Petrosian, V. 1992, in *Statistical Challenges in Modern Astronomy*, Eds. E. D. Feigelson and G. J. Babu, (New York: Springer-Verlag), p. 173.

Press, W. H., Teukolsky, S. A., Vetterling W. T., and Flannery, B. P., 1992. *Numerical Recipes in FORTRAN*. (Cambridge: Cambridge University Press).

Schmidt, M. 1963, Nature, 197, 1040.

Schmidt, M. 1968, Ap.J., 151, 293.

Schmidt, M. and Green, R. F. 1978, Ap.J. (Letters), 220, L1.

Schmidt M., Schneider, D. P. and Gunn, J. E. 1995, A.J., 110, 68.

Shaver, P. A., Hook, I. M., Jackson, C. A., Wall, J. V., and Kellermann, K. I. 1998, to appear in *Highly Redshifted Radio Lines*, eds. C. Carilli, S. Radford, K. Menten, G. Langston, (PASP: San Francisco). astro-ph/9801211.

Siemiginowska, A., and Elvis, M. 1997, Ap. J. (Letters), in press. astro-ph/9703096.

Tananbaum, H., et al. 1979, Ap.J. (Letters), 234, L9.

Tsai, W. 1990, Biometrika, 77, 169.

Warren, S. J., Hewett, P. C., and Osmer, P. S. 1994, Ap.J., 421, 412.